Monthly Notices
of the
ROYAL ASTRONOMICAL SOCIETY

MNRAS **475,** 3029–3045 (2018)
Advance Access publication 2018 January 23

doi:10.1093/mnras/sty048

The star-forming cores in the centre of the Trifid nebula (M 20): from *Herschel* to the near-infrared

M. Tapia,[1]★ P. Persi,[2] C. Román-Zúñiga,[1] D. Elia,[2] F. Giovannelli[2] and L. Sabau-Graziati[3]

[1] *Instituto de Astronomía, Universidad Nacional Autónoma de México, Ensenada, B. C., CP 22830, Mexico*
[2] *INAF–Istituto di Astrofisica e Planetologia Spaziali, Via Fosso del Cavaliere 100, I-00133 Roma, Italy*
[3] *INTA – Instituto Nacional de Técnica Aeroespacial , Ctra. Ajalvir Centro Comerci, Km 4, E-28850 Torrejón de Ardoz, Madrid, Spain*

Accepted 2017 December 25. Received 2017 December 24; in original form 2017 August 17

ABSTRACT

A new detailed infrared (IR) study of eight star-forming dense condensations (TCs) in M 20, the Trifid nebula, is presented. The aim is to determine the physical properties of the dust in such globules and establish the presence and properties of their embedded protostellar and/or young stellar population. For this, we analysed new *Herschel* far-IR and Calar Alto near-IR images of the region, combined with *Spitzer* Infrared Array Camera (*Spitzer*/IRAC) archival observations. We confirm the presence of several young stellar objects (YSOs), most with mid-IR colours of Class II sources in all but one of the observed cores. Five TCs are dominated in the far-IR by Class I sources with bolometric luminosities between 100 and 500 $L_{\odot}$. We report the discovery of a possible counterjet to HH 399 and its protostellar engine inside the photodissociation region TC2, as well as a bipolar outflow system, signposted by symmetric H_2 emission knots, embedded in TC3. The present results are compatible with previous suggestions that star formation has been active in the region for some 3×10^5 yr, and that the most recent events in some of these TCs may have been triggered by the expansion of the H II region. We also obtained a revised value for the distance to M 20 of 2.0 ± 0.1 kpc.

Key words: circumstellar matter – stars: formation – infrared: stars.

1 INTRODUCTION

The Trifid nebula (M 20) is an H II region with an age of approximately 0.3 Myr (Lefloch & Cernicharo 2000) ionized by the O7.5 III star HD164492A (Walborn 1973) located in the Saggitarius spiral arm only a few degrees from the Galactic Centre ($l = 7°, b = 0.25°$). Recent investigations have assumed a distance to M 20 of 1.68 kpc, as derived by Lynds, Canzian & O'Neal (1985). Radio-continuum and CO maps show that its expansion has encountered a large dense molecular cloud to the south-west (SW), possibly triggering the formation of new stars (Cernicharo et al. 1998).

For many decades, the Trifid nebula has been suspected to be an active star-forming centre (Chaisson & Wilson 1975), but the details of how these processes are acting in the region have only been studied in recent years with the advent of satellite missions. The *Infrared Space Observatory* (*ISO*) and *Hubble Space Telescope* (*HST*) observations (Cernicharo et al. 1998; Lefloch & Cernicharo 2000) show the Trifid to be a dynamic star-forming region containing young stellar objects (YSOs), many of them undergoing episodes of violent mass ejection or transferring mass and energy to the nebula in the form of jets.

From millimetre and submillimetre-wavelengths maps, 33 dense cores (TC = Trifid condensation) have been identified, initially by Cernicharo et al. (1998) and Lefloch & Cernicharo (2000), and later extended by Lefloch, Cernicharo & Pardo (2008). Many of these cores show evidence of active star formation. From the *Spitzer* Infrared Array Camera (*Spitzer*/IRAC) and Multi-Band Imaging Photometer for *Spitzer* (MIPS) images of the Trifid nebula (M 20), Rho et al. (2006) listed about 160 YSOs at different evolutionary stages distributed around the whole nebula, and beyond. These cover all stages of proto-stellar evolution, from the early pre-stellar to the late proto-planetary phases. The most conspicuous, likely the youngest, are located within the dense far-IR and millimetre cores.

Evidence of jets and collisions originating from protostars in some of the dense cores have been discovered through narrow-band line imaging in the optical, most conspicuously with the *HST*. Sticking out of the boundaries of one of the cores, TC2 is a 22-arcsec-long irradiated jet HH 399, ending close to a bow shock some 1.5 arcmin away, in a low density environment (Cernicharo et al. 1998; Rosado et al. 1999; Yusef-Zadeh, Biretta & Wardle 2005b). Evidence of shocked gas associated with core TC1 has also been provided by Yusef-Zadeh, Biretta & Geball (2005a).

Finally, Rho et al. (2004) reported the detection of 304 X-ray sources with the *Chandra* satellite, 70 per cent of which having near-infrared (near-IR) counterparts. X-ray emission was detected from

★ E-mail: mt@astrosen.unam.mx

within condensation TC1 and possibly TC4, two star-forming cores with bipolar wings and associated Class 0 candidates (Rho et al. 2004). A recent comprehensive review of the Trifid star-forming region has been presented by Rho et al. (2008).

In order to study in detail the principal star-forming cores within M 20, we present here new far-IR images from the Herschel Infrared Galactic Plane Survey (HI-GAL; Molinari et al. 2010), combined with a new set of deep near-IR images obtained through broad- and narrow-band filters from the Calar Alto 3.5-m telescope. In addition, archival *Spitzer* Infrared Array Camera (IRAC) images (Fazio et al. 2004 ; Werner et al. 2004), part of its Galactic Legacy Infrared Mid-plane Survey Extraordinaire (GLIMPSE) survey (Benjamin et al. 2003), are used to supplement these observations. The observations are described in Section 2, whereas in Section 3, we present the results and discussion. Finally, Section 4 lists our conclusions.

2 OBSERVATIONS AND DATA ANALYSIS

2.1 HI-GAL images and photometry

The Trifid nebula has been observed in the far-IR as part of the *Herschel* satellite (Pilbratt et al. 2010) HI-GAL survey at 70,160, 250, 350, and 500 μm. The images were reduced using the HI-GAL standard pipeline (Traficante et al. 2011). From these, source extraction and photometry were performed using the CUTEX package (Curvature Threshold Extractor), independently at each band (Molinari et al. 2016). Fig. 1 (lower right-hand panel) illustrates the *Herschel* three-colour image of an area of 12 × 12 arcmin^2 around the Trifid nebula, composed from the 70 μm (blue), 160 μm (green), and 250 μm (red) single images.

The brightest dense cores have been associated with those found at millimetre wavelengths (Lefloch et al. 2008) as labelled in Fig. 1. In addition, filamentary structures are present in the nebula. In Table 1, we report the observed *Herschel* fluxes, taken from the catalogues of Molinari et al. (2016), of the five bright dense cores (TC0, TC1, TC2, TC3, and TC4a) that will be discussed in the paper. Note that subcondensations TC4b, TC4c, and TC8 are very faint in several of the Herschel wavelengths, and because of the rather large uncertainties in their measured fluxes, we considered them unreliable for estimating dust masses and temperatures, we opted not to fit modified blackbodies to these TCs.

From the observed *Herschel* flux densities F_ν (Table 1), we constructed the spectral energy distributions (SEDs) of the five aforementioned condensations. We derived masses and dust temperatures for these clumps by fitting single-temperature modified black bodies to their SEDs, following Giannini et al. (2012) and Elia et al. (2013, 2017). This procedure is described and well illustrated by Tapia et al. (2014). Assuming a distance of $d = 2.0$ kpc (see Section 2.2), the derived masses and temperatures for the five dense cores are reported in Table 2.

2.2 Near- and mid-infrared observations and photometry

Near-IR images of M 20 were obtained in service mode with the OMEGA 2000 camera (Kovacs et al. 2004) mounted on the 3.5-m telescope of the Calar Alto Observatory (Centro Astronómico Hispano Alemán, CAHA) atop Sierra de los Filabres in Almería, Spain during the nights of 2013 June 21 and 23. This camera uses a 2K × 2K HAWAII-2 array with a pixel scale of 0.45 arcsec pixel^{-1}. We observed the region with the J, H, and K_s broad-band filters, as well as with two narrow-band filters, H_2 ($\lambda = 2.12$ μm) and Kc (2.144 μm). In each band, we constructed a dithered mosaic of approximately 16 × 16 arcmin^2 around the central position $\alpha(J2000) = 18^h02^m29\overset{s}{.}6$, $\delta(J2000) = -23°00'27''$. The data were processed using adapted versions of the FLAMINGOS reduction and photometry pipelines (Román-Zúñiga 2006; Levine 2008). Both pipelines use a combination of standard IRAF Command Language environment, FORTRAN and IDL routines. The reduction package uses a two-pass sky subtraction technique and an optimized registration using source centroids. The photometry package identifies sources with the SEXTRACTOR algorithm, optimized with the use of a Gaussian convolution filter and 32-level de-blending (Bertin & Arnouts 1996). Point spread function (PSF) magnitudes are calculated with the DAOPHOT algorithms (Stetson 1987). A zero-point calibration and an accurate (<0.05 arcsec rms) astrometric solution were obtained by comparing with existing 2MASS catalogues of the region. In Table 3, we list dates, filters, exposure times, full width at half-maximum (FWHM), and depth values for all observations.

Fig. 1 (upper left-hand panel) illustrates the JHK_s colour-mosaic covering the observed field of the Trifid nebula. The colour-coded image composed of the *Spitzer*/IRAC 3.6, 4.5, and 5.8 μm frames of the same area is also displayed in Fig. 1 (lower left-hand panel).

In order to illustrate the quality of the photometry, we show in Fig. 2 the $J - H$ versus $H - K_s$ diagram of 1570 sources with intrinsic photometric errors smaller than $\sigma_{HK} = 0.07$ and $\sigma_J = 0.03$ (approximate limiting magnitudes were $J = 17.9$, $H = 17.0$, $K_s = 16.8$). These sources lie in two off-nebula circular areas, each of radius 2 arcmin close to the eastern edges of our observed mosaic, some 6 to 7 arcmin from the centre of M 20 and, thus, lie outside the area covered in Fig. 1. These regions, having a total area of $8\pi = 25.1$ square arcmin, appear free of well-defined high-extinction interstellar dust clouds and, thus, are believed to represent the field population in this direction.

The spectroscopic distance determination by Lynds et al. (1985, $d = 1.7$ kpc) has been widely assumed in modern studies of the region. This was based on BV photometry by Hiltner (1956) of the O7.5 III central star HD 164492 A (Walborn 1973; Yusef-Zadeh et al. 2000), assuming dust-reddening properties as determined from the H II line ratios and a value of the total to selective extinction ratio of $R_V = 5.0$. Other values, nevertheless, have been proposed (Stone 1978; Kohoutek, Mayer & Lorenz 1999). In order to revise the value of the distance, we made use of accurate BV published photometry of HD 164492 A by Hiltner (1956), Tapia (1981b), and Kohoutek et al. (1999). Conspicuously, all these determinations agree with each other (within their 2 per cent uncertainty), $V = 7.63$ and $B - V = 0.00$. Note that, when required, the contribution of nearby star HD 164492 B was subtracted. We combined this optical photometry with near-IR JHK_s data from the 2MASS Point Source Catalog (Strutskie et al. 2006), which clearly separates the component A from the other stars of the multiple system ADS 10991. Assuming intrinsic colours and absolute magnitudes in V, J, and K_s of the O7.5 III star by Martins, Schaerer & Hillier (2005) and Pecaut & Mamajet (2013), we obtained: $A_J = 1.39E(V - J) = 0.5$, $A_V = 1.1E(V - K) = 1.3$, and derived $R_V = A_V/E(B - V) = 3.9$. Note that the value of A_V determined by using the J and K_s photometry does not require any assumption on the value of R_V (e.g. Tapia et al. 1988). The revised mean value of the distance to M 20 that we found is $d = 2.0 \pm 0.1$ kpc, which is 18 per cent larger than Lynds et al.'s previous determination. We adopted this new value for the present calculations.

We also performed aperture photometry of all the unresolved *Spitzer*/IRAC sources that were detected within the area of the dark clouds associated with the dense clouds TC0, TC1, TC2, TC3,

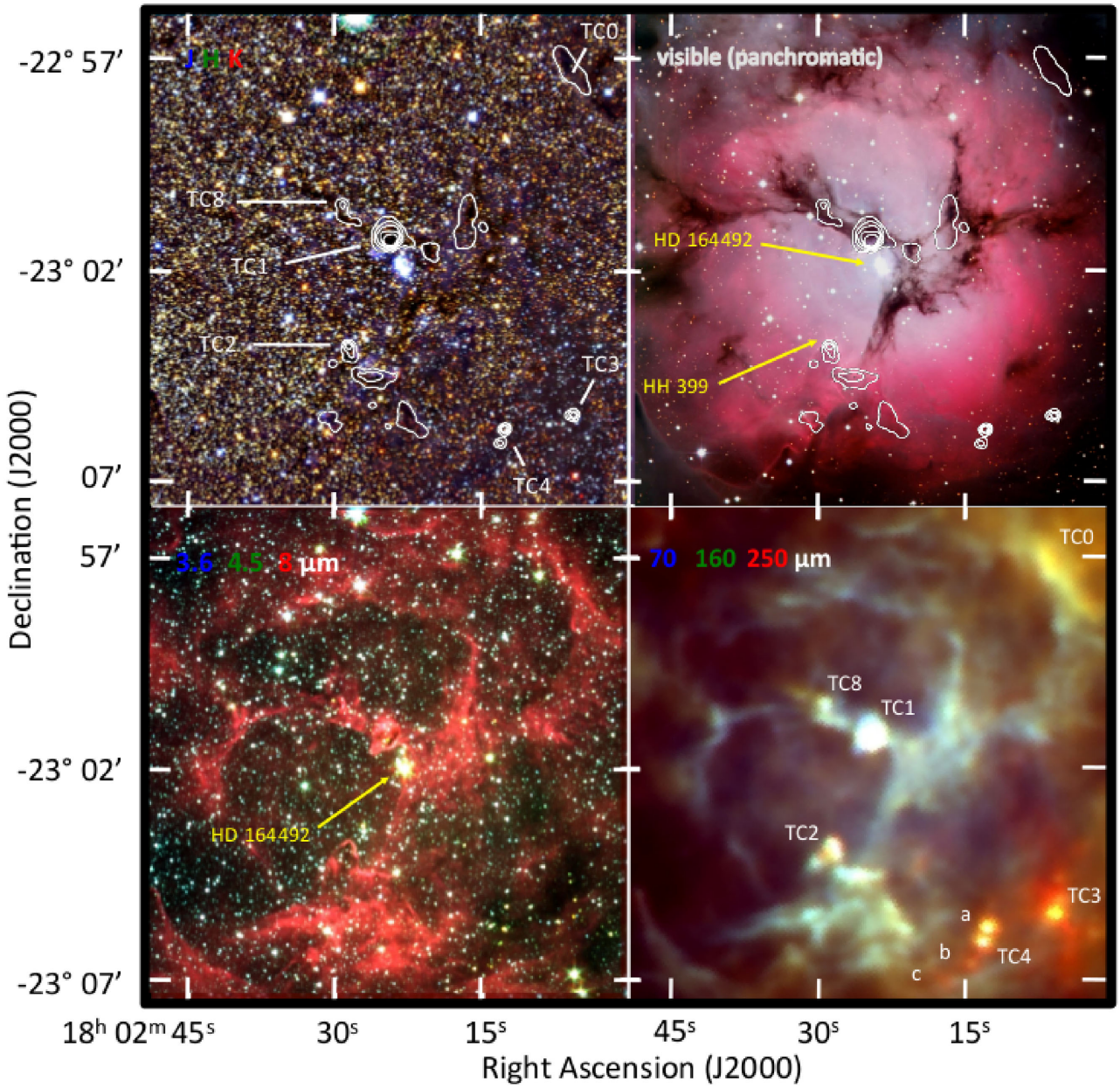

Figure 1. 12 × 12 arcmin^2 (7.0 × 7.0 pc) colour-coded images of the Trifid nebula. Lower right-hand panel: *Herschel* at 70 μm (blue), 160 μm (green), and 250 μm (red); lower left-hand panel: *Spitzer*/IRAC at 3.6, 4.5 and 5.8 μm; upper left-hand panel: CAHA 3.5m in the *JHK*$_s$ bands; upper right-hand panel: a visible public image from the European Southern Observatory. All images have the same scale and are centred at the same position. The white contours are from the *Herschel* 160 μm frame. The white labels indicate the TCs that were studied in this work. The yellow arrows indicate the location of the early-type trapezium system HD 164492, which ionizes the H II region, and the Herbig–Haro jet HD 399 associated with TC2.

Table 1. Flux densities of five dense condensations measured with *Herschel*.

Source	$\alpha(J2000)$ (h m s)	$\delta(J2000)$ (° ′ ″)	F[70] (Jy)	F[160] (Jy)	F[250] (Jy)	F[350] (Jy)	F[500] (Jy)
TC0	18 02 06.6	−22 57 01	–	13.1 ± 1.5	35.0 ± 2.8	18.0 ± 2.1	8.8 ± 1.0
TC1	18 02 24.6	−23 01 17	42.1 ± 5.1	69.8 ± 7.0	114.5 ± 11.2	41.8 ± 5.0	16.4 ± 1.8
TC2	18 02 28.5	−23 03 49	41.6 ± 4.8	69.8 ± 7.2	66.8 ± 5.9	22.6 ± 2.7	8.0 ± 1.1
TC3	18 02 05.7	−23 05 27	7.7 ± 1.3	34.2 ± 3.8	77.1 ± 7.1	39.4 ± 3.6	20.5 ± 2.1
TC4a	18 02 12.7	−23 05 46	23.2 ± 2.5	38.0 ± 4.0	99.7 ± 10.0	45.5 ± 5.1	20.5 ± 2.0

Table 2. Masses and temperatures of the dense cores.

Dense core	M ($M_\odot$)	T_d (K)
TC0	129	13.0
TC1	149	16.0
TC2	53	18.8
TC3	255	14.8
TC4a	148	17.8

Table 3. Calar Alto Near-IR observations of M 20.

Obs. date	Filter	T_{exp} (sec)	No. frames	FWHM (arcsec)	BD peak (mag)
2013-06-21	J	60.0	10	1.37	18.8
2013-06-21	H	40.0	10	1.35	16.3
2013-06-21	K_s	20.0	10	1.21	17.0
2013-06-23	H_2	60.0	10	1.44	18.0
2013-06-23	K_{cont}	40.0	10	1.26	18.3

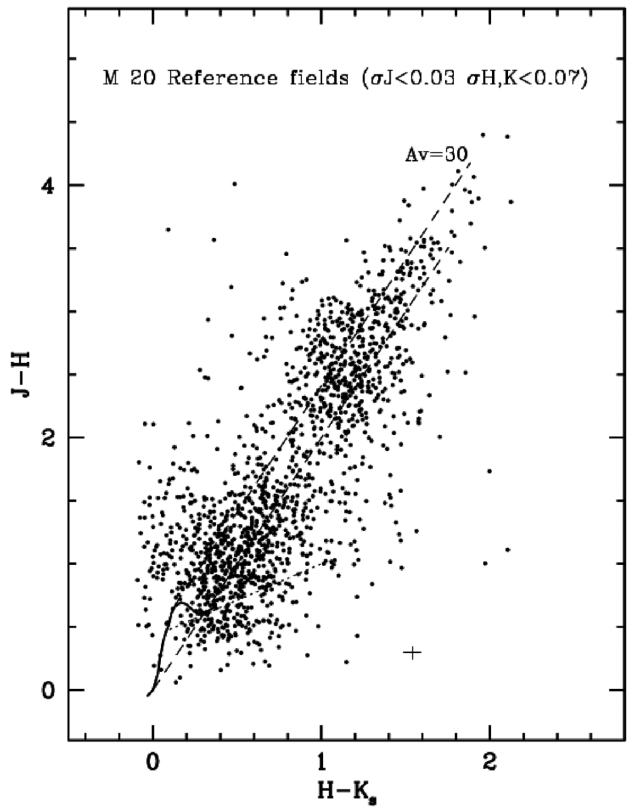

Figure 2. $J - H$ versus $H - K_s$ diagram of two reference regions outside the Trifid nebula. These lie within the field of view of our CAHA JHK_s images, close to the eastern limit. The coordinates of these reference fields are $\alpha(J2000) = 18^h02^m51\overset{s}{.}3$, $\delta(J2000) = -22°55'12''$ and $\alpha(J2000) = 18^h02^m52\overset{s}{.}1$, $\delta(J2000) = -23°02'04''$. The locus of the unreddened stellar photospheres is drawn with a curved solid line (Tokunaga 2000) and the reddening vectors (Rieke & Lebofsky 1985) are shown with dashed lines. The small plus sign illustrates the maximum photometric errors.

TC4a,b,c, and TC8 with the PHOT IRAF package. We set an aperture of 2.4 arcsec with the sky determined by an external ring of 3 arcsec width. As we aimed at measuring the brightness of the stellar source, we managed to subtract as best as possible the diffuse emission that is considerable at 5.8 and 8 μm. Because of this, very few compact sources could be measured in these two IRAC bands. The estimated maximum uncertainty in the [3.6] and [4.5] magnitudes is 0.1, whereas for the longer wavelengths is 0.15. Appropriate aperture corrections (IRAC Manual[1]) were applied. This photometry was checked with that given by Rho et al. (2006) for a small number of isolated common stars with no diffuse (e.g. polycyclic aromatic hydrocarbon – PAH) emission around, showing no differences beyond the photometric uncertainties.

The results of the OMEGA2000 JHK_s and the IRAC photometry of all compact sources associated with the TCs are given in Table 4. This table also gives the centres and radii of the areas selected for our photometric survey in each TC. The two-colour and colour–magnitude diagrams corresponding to the JHK_s and IRAC photometry in each dense core are presented in Figs 3–6. In Fig. 7, we present the 1 to 1000 μm SEDs of the most conspicuous class I YSO in TC1, TC2, TC3, and TC4a, all discussed in Section 3.2–3.6.

3 RESULTS AND DISCUSSION

A total of 32 protostellar Class 0/I and around 120 Class II candidates have been proposed by Rho et al. (2006) and Lefloch et al. (2008) in a large area that extends well beyond the limits of the optical and radio H II region. However, here we concentrate on reanalysing the IR properties of the densest dust cores located within a radius of 6 arcmin from the HD 164492A, namely TC0, TC1, TC2, TC3, TC4a,b,c, and TC8. In particular, we pay attention to study the presence and properties of the associated embedded stellar and/or protostellar population, outflow engines, and masses and dust temperatures of the cores. For this, we limit the areas of our photometric near- and mid-IR study to those of the projected size of the near-IR dark cloud and far-IR *Herschel* emission, in many cases also delineated by 5.8 and 8 μm-bright PAHs on the *Spitzer* images. The results for each of the eight cores will be presented and discussed in the following section.

Figs 8 to12 display collages of close-up (size 143 × 113 arcsec) sections of the IR images of the principal dense cores described in this paper, TC0, TC1/TC8, TC2, TC3, and TC4a,b,c, respectively. Each figure includes colour-composite images constructed from our CAHA JHK_s frames (upper left-hand panel), the *Spitzer*/IRAC 3.6, 4.5, and 8 μm frames (upper right-hand panel), the *Herschel* 70, 160, and 250 μm frames (lower left-hand panel), and the grey-scale continuum-subtracted narrow-band H_2 image (lower right-hand panel). All panels have the same scale and orientation and provide a helpful visualization aid to the physical conditions determined quantitatively by means of multiwavelength photometry listed in Tables 1 and 4.

3.1 The trifid condensation TC0

According to Lefloch et al. (2008) based on 1.25 mm-wavelength observations, TC0 is a dense starless core, with $n_e \simeq 10^5 cm^{-3}$. It is currently being hit by the ionization front from HD 16449A, and is thought to be the site for the formation of the next generation of

[1] http://irsa.ipac.caltech.edu/data/SPITZER/docs/irac/iracinstrumenthandbook/90/

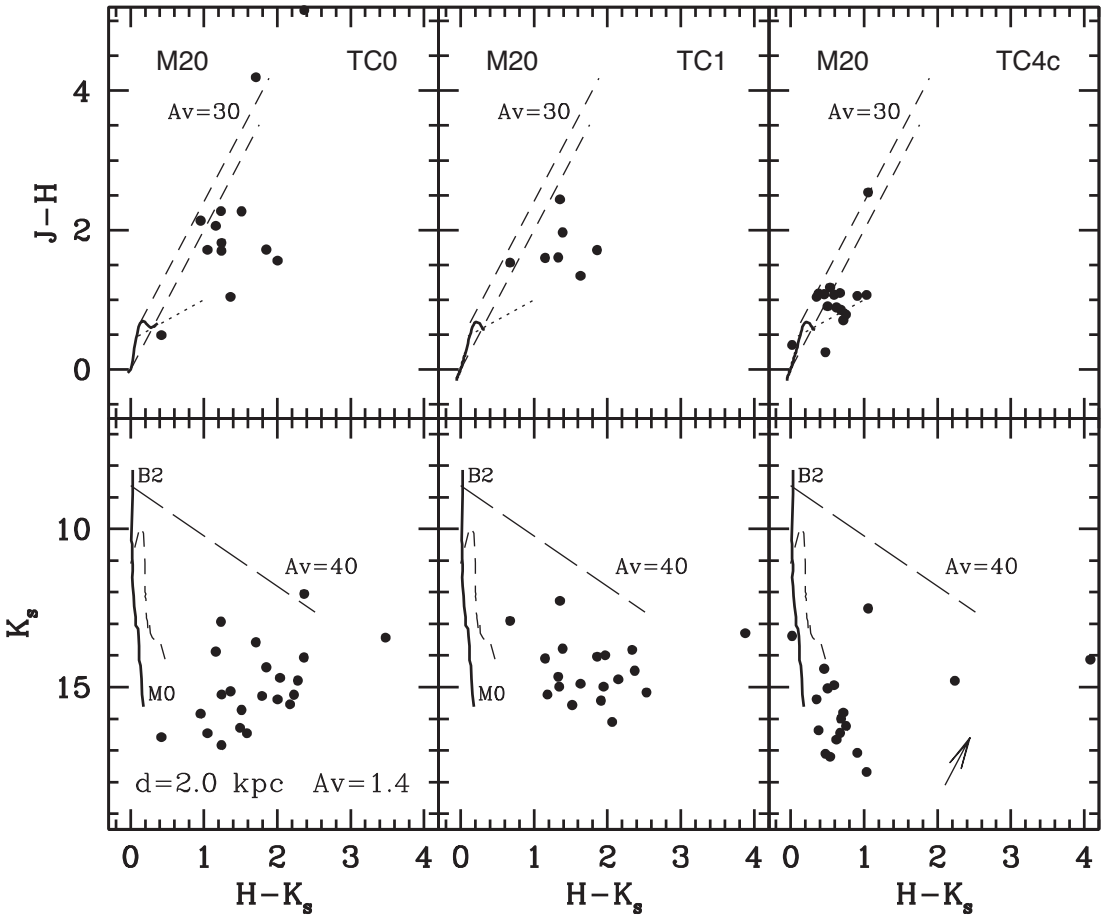

Figure 3. $J-H$ versus $H-K_s$ (upper panels) and K_s versus $H-K_s$ diagrams (lower panels) of all sources with measured HK_s photometry in each of the TC0, TC1, and TC4c fields in central M 20 (see text). In each of the two-colour diagrams, the locus of the unreddened stellar photospheres is drawn with a curved solid line (Tokunaga 2000) and, with dotted lines, which are occupied by unreddened Classical T Tauri stars (Meyer, Calvet & Hillebrand 1997). In each of the colour–magnitude diagram, the main sequence for a distance of $d = 2.0$ kpc and foreground $A_V = 1.4$ is represented by a continuous line, whereas the dashed line represents the 1 Myr isochrone from Siess, Dufour & Forestini (2000). The arrow indicates the shift caused by pre-main-sequence discs (López-Chico & Salas 2007). In all diagrams, the reddening vectors (Rieke & Lebosky 1985) are shown as straight broken lines

stars in the region. Fig. 8 displays the 1.2–250 μm morphology of the TC0 region from our observations. The far-IR to millimetre dust emission appears elongated in the SW to NE direction with several local maxima. This, together with the IRAC PAH-dominated 8 μm emission, traces the boundary between the expanding H II region and the photodissociation region (PDR) created in the perturbed dense cloud. This structure appears very similar to that mapped in the ^{12}CO and ^{13}CO(1–0) emission lines by Lefloch et al. (2008; their fig. 2). The dust temperature of the core, derived from the *Herschel* fluxes (Table 2), is the lowest of the region ($T_{\rm dust} = 13$ K), and its total mass (assuming a gas-to-dust ratio of 100) is 129 $M_\odot$.

Our near-IR photometry (Table 4 and Fig. 5) does not reveal any star with excess emission at $\lambda > 2$ μm that appear to be inside the dark cloud, confirming the starless nature of the core. Of the two stars with IRAC colours of Class II objects, one (TC0-1) has JHK_s colours of a lowly reddened photosphere indicating that it is not embedded in the dense cloud, whereas the other (TC0-2) lies on the edge of the cloud. Similarly, a number of red (in the near-IR) stars appear to be highly reddened low- and mid-luminosity pre-main sequence (Class II) stars located outside the dark cloud, and thus are probable members of the M 20 cluster but clearly unrelated to TC0 (Fig. 8). Finally, from the narrow-band near-IR images, we did not detect any H_2 knots in the TC0 cloud. All these results are in agreement with the results by Lefloch et al. (2008) and Rho et al. (2008), who concluded that TC0 is a pre-stellar core.

3.2 The trifid condensation TC1

Of all the dense cores in M 20, TC1 is closest to the centre of the H II region, located only some 50 arcsec to the north-west (NW) of HD 164492A, the O7.5 star responsible for providing most of the ionizing UV photons to the whole nebula. The warm-dust millimetre and far-IR *Herschel* emission is nearly circular. Lefloch et al. (2008) reported a peak hydrogen gas column density of 1.6×10^{23}cm^{-2} in this condensation. For a central dense core of size 0.16 pc, its mean density is, therefore, 1.8×10^5cm^{-3}. From the optical depth of the silicate feature, these authors obtained a peak value of $A_V = 145$.

Our *Herschel* fluxes yield a dust mass of 149 $M_\odot$ and $T_{\rm dust}$ of 16 K. In the near-IR, it appears as a sharp-edged dark cloud of 30 arcsec diameter. Clearly, this PDR is being photoionized by HD 164492A. This star's strong radiation produces a very sharp bright rim along the southern edge of the dense TC1 globule facing the ionizing star. This is best appreciated on the composite [O III], Hα, [S II] *HST* image presented in fig. 2 of Yusef-Zadeh et al. (2005a), and is also evident on the present J-band and H_2 images (Fig. 9). The observed morphology of the rim strongly suggests that the

Table 4. Centre and radii of the observed fields TC0, TC1, TC2, TC3, TC4a, TC4b, TC4c, and TC8 with coordinates, photometry, identification, and classification of compact sources.

$\alpha(J2000)$ (h m s)	δ (J2000) (° ′ ″)	J (mag)	H (mag)	K_s (mag)	[3.6] (mag)	[4.5] (mag)	[5.8] (mag)	[8] (mag)	ID	Notes
18 02 06.30	−22 57 00.2	TC0	$r = 20$ arcsec							
18 02 05.88	−22 57 09.8	16.44	14.16	12.93	11.35	10.58	10.23	9.00	1	Class II
18 02 06.80	−22 57 18.8	–	16.91	13.43	11.02	10.64	10.13	10.85	2	Class II
18 02 07.05	−22 57 14.9	19.48	15.29	13.58	12.39	12.33	–	–	3	OB star
18 02 07.15	−22 57 09.0	19.57	14.42	12.05	10.48	10.17	10.04	9.87	4	OB star
18 02 05.48	−22 57 06.2	19.50	17.23	15.72	14.98	14.96	–	–	5	
18 02 05.32	−22 56 51.8	19.22	17.51	16.46	15.04	14.32	–	–	6	
18 02 06.37	−22 56 47.5	20.26	17.07	15.28	13.84	13.61	–	–	7	
18 02 07.31	−22 57 02.7	–	17.71	15.54	14.77	14.84	–	–	8	
18 02 05.40	−22 56 58.9	–	17.07	14.79	13.37	13.32	–	–	9	
18 02 07.19	−22 56 54.3	–	16.42	14.06	12.56	12.31	12.10	–	10	OB star
18 02 06.22	−22 56 45.8	–	–	16.23	13.84	13.49	–	–	11	
18 02 05.60	−22 56 53.4	–	–	16.22	14.55	14.11	–	–	12	
18 02 06.10	−22 56 55.1	–	–	17.59	14.56	13.51	–	–	13	
18 02 06.71	−22 57 01.0	–	–	16.96	14.02	13.01	12.89	–	14	
18 02 06.92	−22 57 01.5	–	–	17.08	14.32	14.44	–	–	15	
18 02 06.83	−22 57 15.0	17.10	15.04	13.87	12.39	14.15	–	–	16	
18 02 07.04	−22 57 03.0	–	16.49	15.13	14.30	14.01	–	–	17	
18 02 07.46	−22 56 59.7	–	16.48	15.23	13.05	12.87	–	–	18	
18 02 05.48	−22 57 06.2	19.50	17.23	15.72	–	–	–	–	19	
18 02 07.65	−22 56 59.2	17.94	16.22	14.37	13.18	12.94	–	–	20	OB star
18 02 24.84	−23 01 12.0	TC1	$r = 20$ arcsec							
18 02 23.90	−23 01 21.3	16.85	15.25	14.10	12.16	11.89	9.70	–	1	
18 02 24.37	−23 00 56.0	17.14	15.17	13.79	12.31	11.68	10.71	10.19	2	Class II
18 02 24.49	−23 01 13.7	–	17.34	15.43	13.47	13.11	11.30	–	3	
18 02 24.61	−23 01 03.6	16.06	13.62	12.27	11.28	10.94	10.51	–	4	Class II
18 02 24.69	−23 00 43.8	–	–	–	12.76	9.98	8.74	8.68	6=A	Class I
18 02 24.92	−23 01 10.0	–	15.96	13.99	12.13	11.71	11.20	–	7	Class II
18 02 24.99	−23 01 01.2	17.24	16.93	14.99	13.04	13.10	10.67	9.79	8	
18 02 25.06	−23 00 57.0	–	16.16	13.82	12.03	11.64	10.39	10.73	9	
18 02 25.08	−23 01 19.5	–	17.17	13.29	10.23	9.52	9.23	10.09	10=B	Class II
18 02 25.16	−23 01 26.6	17.61	15.89	14.03	11.62	10.85	10.07	9.21	11=C	Class II
18 02 25.63	−23 00 56.8	15.11	13.58	12.90	12.37	12.36	–	–	13	
18 02 25.82	−23 01 03.7	–	16.85	14.48	12.76	12.38	10.68	9.75	15	
18 02 25.76	−23 01 27.4	17.87	16.53	14.89	13.44	13.37	–	–	16	OB star
18 02 24.85	−23 00 54.8	18.58	17.08	15.56	13.95	14.36	–	–	18	
18 02 25.42	−23 01 24.3	–	16.42	15.23	14.04	13.72	–	–	19	
18 02 26.23	−23 01 15.6	–	16.90	14.76	13.39	13.15	–	–	20	
18 02 26.13	−23 01 09.4	–	17.70	15.17	13.01	12.99	–	–	21	
18 02 26.26	−23 01 10.4	–	18.17	16.10	12.87	12.31	–	–	22	
18 02 28.76	−23 04 00.2	TC2	$r = 20$ arcsec							
18 02 27.55	−23 03 59.0	15.61	11.96	10.15	9.24	9.12	9.01	9.08	1	OB star
18 02 28.45	−23 04 03.0	–	–	–	13.77	12.93	12.50	–	2	Class II
18 02 28.46	−23 04 14.9	–	16.85	15.17	13.73	13.60	12.29	11.15	3	
18 02 28.50	−23 03 57.2	19.24	15.77	13.68	11.86	11.47	11.02	9.56	4	Class II
18 02 28.65	−23 04 17.9	18.49	14.29	12.48	11.31	11.31	11.14	11.13	5	OB star
18 02 28.62	−23 03 48.3	–	–	–	14.90	13.31	12.42	11.63	6=A	Class I
18 02 28.89	−23 03 55.1	16.97	14.10	12.62	11.43	11.31	11.12	10.26	7	OB star
18 02 28.91	−23 04 18.7	15.60	14.03	13.16	12.24	11.83	11.56	10.36	8	
18 02 29.00	−23 04 12.1	–	15.59	13.02	10.99	10.73	10.54	10.11	9	OB star
18 02 29.20	−23 03 53.7	–	17.90	16.03	14.68	14.22	–	–	10	
18 02 29.43	−23 03 57.5	16.62	14.97	13.94	13.18	13.23	–	–	11	
18 02 29.49	−23 04 02.5	18.72	13.92	11.57	9.92	9.69	9.33	9.42	12	OB star
18 02 29.56	−23 04 09.1	14.90	12.10	10.76	9.79	9.62	9.62	9.29	13	OB star
18 02 29.95	−23 04 03.8	–	17.35	14.66	13.42	13.24	–	–	14	
18 02 29.95	−23 03 51.3	14.42	13.34	12.99	11.44	12.09	–	–	15	
18 02 25.87	−23 04 36.2	–	16.60	13.87	12.31	11.80	11.50	–	16	Class II
18 02 28.21	−23 03 58.4	–	17.4	15.8	12.5	12.3	12.3	–	17	H_2 knot
18 02 05.67	−23 05 26.5	TC3	$r = 20$ arcsec							
18 02 05.22	−23 05 28.2	11.36	11.05	10.97	10.94	10.99	–	–	1	
18 02 04.90	−23 05 21.1	–	–	15.86	11.87	11.08	10.35	10.43	2	Class II

Table 4 – *continued*

α (*J*2000) (h m s)	δ (° ′ ″)	*J* (mag)	*H* (mag)	K_s (mag)	[3.6] (mag)	[4.5] (mag)	[5.8] (mag)	[8] (mag)	ID	Notes
18 02 05.29	−23 05 35.9	13.61	12.90	12.80	12.62	12.84	–	–	3	
18 02 05.57	−23 05 29.0	–	–	–	12.68	10.08	8.63	7.85	4=A	Class I
18 02 06.70	−23 05 36.3	13.86	12.47	11.94	11.56	11.53	11.77	12.43	5	
18 02 06.03	−23 05 45.8	14.52	13.20	12.77	12.33	12.33	–	–	6	
18 02 06.12	−23 05 27.7	16.12	14.99	14.54	–	–	–	–	7	
18 02 04.56	−23 05 29.1	17.36	16.54	15.86	13.24	12.24	11.55	11.50	8	
18 02 07.19	−23 05 36.1	–	–	14.06	11.10	8.81	8.17	8.22	9=B	Class II
18 02 07.08	−23 05 37.4	–	–	14.06	10.50	9.71	9.09	9.12	10	
18 02 05.43	−23 05 5.4	–	–	16.25	11.63	9.84	9.09	8.52	11=C	Class II
18 02 12.86	−23 05 56.4	TC4a	$r = 20$ arcsec							
18 02 12.75	−23 05 46.7	16.76	15.46	13.50	10.56	8.60	7.16	6.15	1=A	Class I
18 02 12.48	−23 05 48.7	18.10	14.88	13.16	11.19	10.36	–	–	2	OB star
18 02 12.58	−23 05 45.9	–	14.61	12.93	10.67	–	–	–	3	
18 02 13.09	−23 06 06.9	–	–	15.60	12.05	10.36	10.11	–	4=B	Class II
18 02 12.26	−23 05 44.6	–	16.00	13.92	12.45	11.68	11.11	–	5	Class II
18 02 13.71	−23 05 49.5	–	–	15.70	13.46	12.57	–	–	6	
18 02 12.47	−23 05 41.3	–	17.25	14.64	13.40	12.74	12.03	–	7	Class II
18 02 11.94	−23 05 49.3	–	–	16.46	13.90	12.78	12.00	–	8	Class II
18 02 13.02	−23 06 04.7	–	17.17	15.81	–	–	–	–	9	
18 02 14.23	−23 06 36.0	TC4b	$r = 15$ arcsec							
18 02 14.02	−23 06 30.0	–	16.27	13.61	11.74	11.51	11.37	–	1	Class II
18 02 14.03	−23 06 40.4	–	–	–	12.16	10.33	9.55	9.39	2=D	Class I
18 02 13.26	−23 06 31.3	15.83	14.77	14.31	12.37	11.23	10.75	–	3	
18 02 14.01	−23 06 34.3	–	16.90	14.85	13.02	12.30	12.03	–	4	Class II
18 02 13.50	−23 06 44.2	14.29	13.32	12.89	12.55	12.53	12.57	–	5	
18 02 14.37	−23 06 38.1	–	–	–	15.60	12.22	11.03	10.45	6	Class I
18 02 15.77	−23 06 43.2	–	–	14.51	9.45	8.26	7.47	7.51	7=E	Class II
18 02 16.78	−23 07 02.6	TC4c	$r = 15$ arcsec							
18 02 16.85	−23 07 10.4	16.11	13.57	12.51	11.61	11.55	11.79	11.51	1	
18 02 17.16	−23 07 13.8	–	18.21	14.13	11.70	11.18	10.71	10.53	2	Class II
18 02 16.75	−23 07 01.3	13.75	13.40	13.38	13.37	13.31	–	–	3	
18 02 17.52	−23 07 13.4	–	17.03	14.80	13.06	12.19	12.13	–	4	
18 02 17.68	−23 07 17.4	–	16.78	12.13	9.21	8.91	8.69	8.23	5	Class II
18 02 28.73	−23 00 41.8	TC8	$r = 20$ arcsec							
18 02 28.51	−23 00 38.1	12.94	11.68	11.14	9.72	9.14	8.83	7.67	1	Class II
18 02 28.73	−23 00 57.4	16.32	12.11	9.90	8.29	8.29	7.97	8.05	2	OB star
18 02 27.57	−23 00 42.8	17.94	14.02	12.03	10.28	9.77	9.34	9.28	3	Class II
18 02 30.15	−23 00 39.5	12.95	11.48	10.58	9.89	9.78	9.76	9.20	4	
18 02 28.73	−23 00 30.8	–	14.56	12.61	11.22	11.13	11.30	–	5	
18 02 28.42	−23 00 26.3	16.88	14.62	12.89	11.62	11.49	11.46	–	6	OB star
18 02 29.13	−23 00 40.5	16.34	14.13	12.68	11.34	11.37	11.15	–	7	OB star
18 02 29.55	−23 00 54.7	16.70	14.15	12.74	11.55	11.47	11.05	–	8	Class II
18 02 29.83	−23 00 34.1	–	16.13	13.81	12.23	12.03	11.85	11.98	9	
18 02 28.12	−23 00 41.6	18.79	15.19	13.42	12.15	11.99	12.25	–	10	OB star
18 02 28.07	−23 00 37.7	15.17	13.75	13.07	12.26	11.82	11.40	–	11	
18 02 28.52	−23 00 47.2	18.49	15.56	13.79	12.31	11.81	–	–	12	OB star
18 02 28.63	−23 00 33.6	–	16.30	14.43	12.43	12.25	13.65	–	13	
18 02 29.19	−23 00 29.9	–	16.32	14.98	12.17	12.53	8.44	7.75	14	
18 02 29.93	−23 00 36.0	–	17.93	15.79	13.28	12.04	11.86	–	15	
18 02 29.41	−23 00 20.9	–	16.66	13.57	10.32	10.23	10.01	–	16	OB star

illumination comes from the back of the cloudlet, i.e. with TC1 located somewhat closer to the observer than HD 164492A. On the other hand, this core appears wholly delimited by strong PAH emission at 5.8 and 8 μm. Its morphology reveals oval extensions to the south-east (SE) and north that our *Herschel* 70 μm images show to be filled with low-density warmer dust (Fig. 9).

A single, small shocked H_2 emission knot is located inside the SE sub-lobe. Its location coincides with a similar Hα and [S II] emission knot on the *HST* image by Yusef-Zadeh et al. (2005a). Its driving source is unknown at present, but a likely candidate would be an embedded young star, TC1-16, with considerable near-IR excess (and invisible in the *HST* image), only 2 arcsec (0.02 pc) to the north-east (NE) or, alternatively, the low-luminosity Class II star, TC1-11=C, located some 5 arcsec (0.05 pc) to the west. Both are identified in Fig. 9.

As pointed out by Lefloch et al. (2008), a mid-IR source (TC1-6=A), undetected at $\lambda < 2.5$ μm, is located close to the far-IR emission peak (Fig. 9; see also fig. 6 from Lefloch et al. 2008).

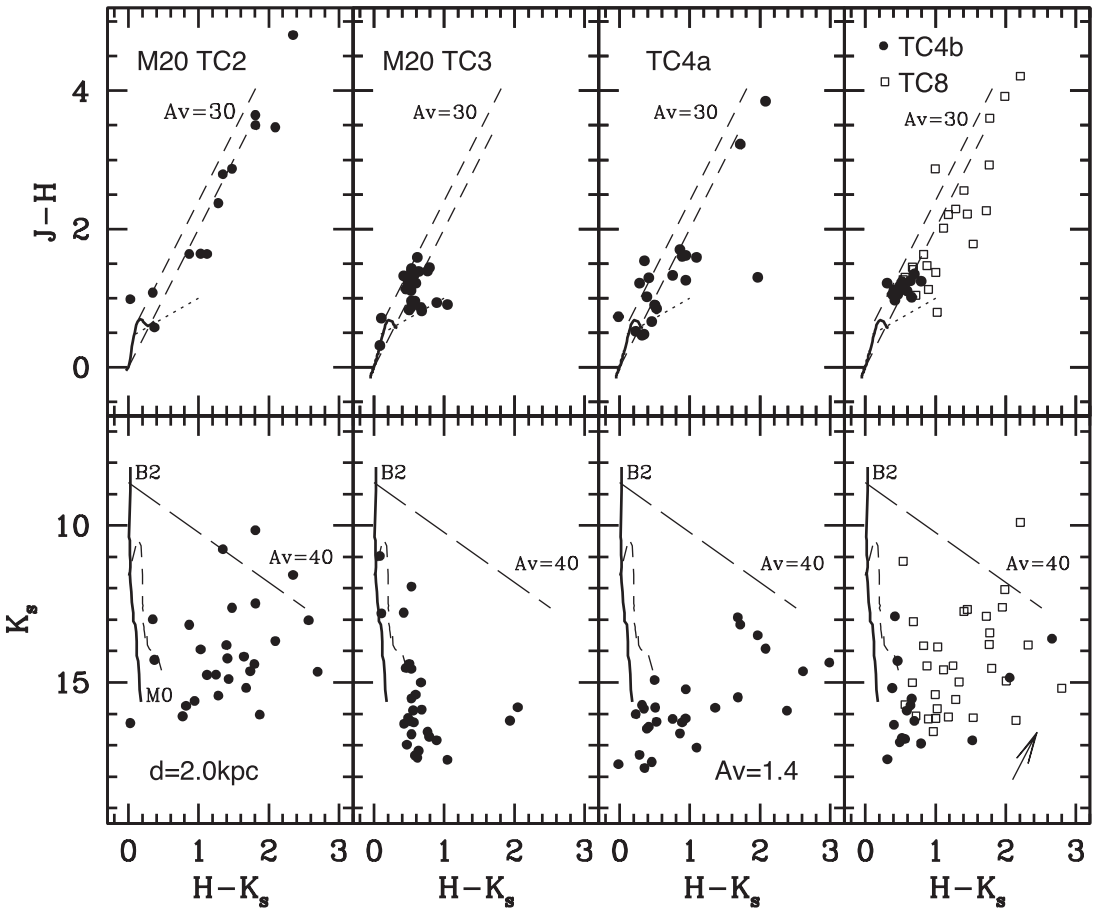

Figure 4. $J - H$ versus $H - K_s$ (upper panels) and K_s versus $H - K_s$ diagrams of all sources with measured HK_s photometry in the each of the TC2, TC3, TC4a, TC4b, and TC8 fields (see text). All illustrative graphics are as in Fig. 3.

Table 5. Physical parameters of the protostellar objects TC1-A, TC2-A, TC3-A, and TC4a-A corresponding to the best two fits of the model of Robitaille et al. (2007) with $\chi^2 - \chi^2_{\rm best} < 3$.

Parameters	TC1-A	TC2-A	TC3-A	TC4a-A
Stellar mass ($M_\odot$)	7.7 7.3	3.4 7.1	5.1 2.1	1.0
Stellar temperature (K)	4603 4773	4299 4389	4497 4497	3974
Envelope accretion rate (10^{-4} $M_\odot$ yr^{-1})	16.2 15.2	9.6 13.3	9.4 9.4	3.3
Disc mass (10^{-3} $M_\odot$)	47.8 4.3	84.9 56.2	153 153	90.2
Disc accretion rate (10^{-7} $M_\odot$ yr^{-1})	6.5 1.6	346 8.1	45.5 45.5	322
A_V	55.4 20.0	23.7 31.5	59.3 20.0	26.0
$L_{\rm bol}$ ($L_\odot$)	568 414	287 444	182 182	110
Inclination angle (degrees)	41 49	32 49	56 63	18

Its IRAC colours indicate that it is a Class 0/I object and its SED (Fig. 7) has been fitted with an infalling envelope+disc+central source radiative transfer model (Robitaille et al. 2006) by using the most recent fitting tool of Robitaille et al. (2007). The best fit for source A yields a luminosity of 568 $L_\odot$ with a 0.05 $M_\odot$ disc reddened by $A_V = 55$. The main parameters for which the best two fits (those with $\chi^2 - \chi^2_{\rm best}$ per data point <2) to the model were obtained are listed in Table 5 and plotted in Fig. 7. This intermediate-mass protostar seems to be the only one presently being formed in the TC1 core.

Several other young stars, including Class II sources TC1-2, TC1-4, TC1-7, TC1-10=B, and TC-1-11=C, the latter also an X-ray source (Rho et al. 2004), are located within the TC-1 dense core (see Table 4 and Fig. 9) and may be sub-products of the strong winds and radiation from the multiple early-type stellar system HD 164492 compressing material into the dense globule.

3.3 The trifid condensation tC2

Rho et al. (2008) described TC2 as a perfect example of a photoionized star-forming globule'. In common with TC1, the surface of the dense dark cloud facing the O-type trapezium stellar system HD 164492 is illuminated by it, thus creating a photodissociation front. This is clearly delineated by PAHs and H_2 fluorescent emission, mainly at 8 and 2.12 μm (Fig. 10), and shown in exquisite detail in the *HST* optical Hα and [S II] lines image by Hester et al. (2004).

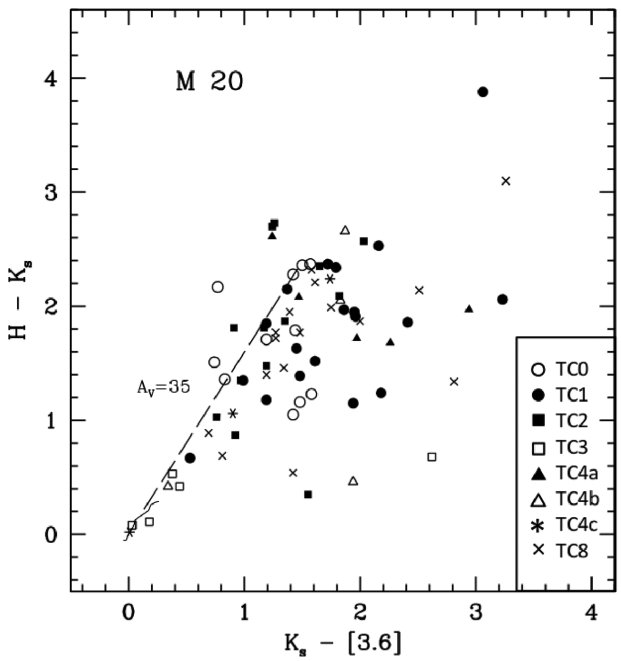

Figure 5. $H - K_s$ versus $K_s - [3.6]$ diagram of all sources with IRAC photometry in the studied TCs in central M 20 as listed in Table 4. The locus of the unreddened stellar photospheres is drawn with a curved solid line and the reddening vector (Tapia 1981a) is shown as a broken line. The legend indicates which symbols refer to which TC.

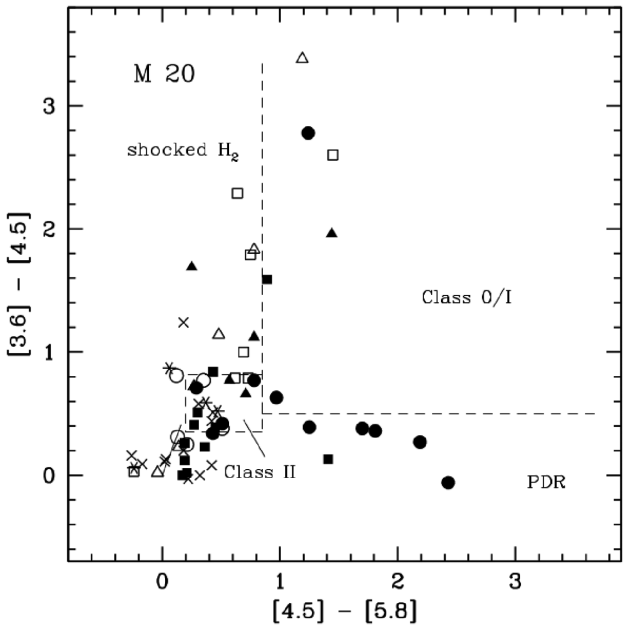

Figure 6. [3.6] − [4.5] versus [4.5] − [5.8] diagram of all sources with IRAC photometry in the studied TCs as listed in Table 4. Broken lines delineate the areas that are occupied by Class 0/I and Class II objects, and also indicated with labels are the approximate zones occupied by shocked H_2- and PAHs-dominated emission regions (Ybarra et al. 2014). Symbols are as in Fig. 5.

These authors also studied the properties of a highly collimated jet, named HH 399, protruding to the NE from the surface of the dark globule (for details, see Cernicharo et al. 1998, Rosado et al. 1999; Hester et al. 2004; Yusef-Zadeh et al. 2005b). Its (proto)stellar engine clearly is embedded deep within the cloud. The jet is also seen in our *J*-band image (Fig. 10), probably because of the emission of the [Fe II] line (see upper panels of Fig. 13). Still, no trace of the jet is seen in the continuum-subtracted H_2 image. A detailed multiwavelength study of this PDR has been published by Lefloch et al. (2002).

From our *Herschel* photometry, we estimate a mass 53 $M_\odot$ for this clump, which makes it the least massive of the central Trifid cores, with a dust temperature of 19 K (Table 2). These values are consistent with the parameters listed by Rho et al. (2008) in their review of M 20. Within the boundaries of TC2, 15 unresolved mid-IR IRAC sources were detected (Fig. 10 and Table 4). Most are bright enough to be measured in the near-IR. Analysis of our photometry (Table 4 and Figs 4 and 5) indicates that six of them are OB-type stars deeply embedded in the clump, with their respective A_V in excess of 20 magnitudes, and no significant mid-IR excess. Two other bright mid-IR sources (TC2-2 and 4 in Table 4) have colours consistent with them being Class II YSOs. The physical and chemical properties of the globule TC2 are described in detail by Lefloch et al. (2002) and summarized in table 2 of Rho et al. (2008).

Of particular interest is the unresolved mid-IR source TC2-6=A (Table 4 and Figs 10 and 13), which was detected only at $\lambda >$ 3 μm (Table 4). Its position at $\alpha(J2000) = 18^h02^m28\overset{s}{.}6$, δ(J2000) $= -23°03'48''$ is, within the uncertainties (∼1 arcsec), that of the *Herschel* far-IR peak emission TC2 (Table 1). Its measured IRAC colours correspond to a Class I YSO (Table 4 and Fig. 6), and has a total IR luminosity of around 300–450 $L_\odot$ (Table 5). It is important to note the peculiar properties of source TC2-17 at $\alpha(J2000) = 18^h02^m28\overset{s}{.}22$, $\delta(J2000) = -23°03'58\overset{''}{.}4$. It appears unresolved in all broad-band images, from 1.6 to 4.5 μm and was undetectable at longer wavelengths. In contrast, it appears very bright and extended (with approximate size 2 × 4 arcsec^2) in the 2.12 μm H_2 line, as is evident in the continuum-subtracted molecular hydrogen images in Figs 10 and 13. This source will be referred to as 'H_2 knot'. Its compactness and location suggest that the line emission originates from shocks, as opposed to the very extended fluorescent molecular hydrogen and PAH emission that delineates the northern border of the PDR in the direction of the hot stars to the north.

From a detailed analysis of the image shown in Fig. 13, we note that the H_2 knot, the whole jet HH 399, and the far- and mid-IRs source TC2-6=A are aligned. It is natural to postulate that the Class I YSO source TC2-6 is the true central engine driving, towards the NE, the HH 399 jet (marked n to m in Fig. 13 and Table 6) that becomes optically bright as it emerges from the interface between the dense PDR and the low-density ambient medium outside. In the opposite direction, a highly reddened counterjet (not yet detected) interacts with the dense material inside the clump, producing the observed small shocked H_2 knots (labelled x, y, z in Fig. 13 and Table 6). The average position angle of the optical HH 399 jet is 19 °, whereas the position angle measured from the southern tip of the jet (on the edge of the PDR) to the H_2 knot (passing through the position of source TC2-6, the central YSO) is 25 °. The difference between these angles may be the result of a kind of 'mechanical refraction' such as that discussed by Raga & Cantó (1995) when a jet passes through the boundary between two media of very different densities. This can lead to complex jet kinematics as seen in HH 399 (Yusef-Zadeh et al. 2000). The measured positions of the knots are listed in Table 6. Note that the angular distance between the proposed central YSO (TC2-6=A) and the southern tip (z) of the proposed H_2 counterjet is 19.7 arcsec (0.19 pc), nearly the same as

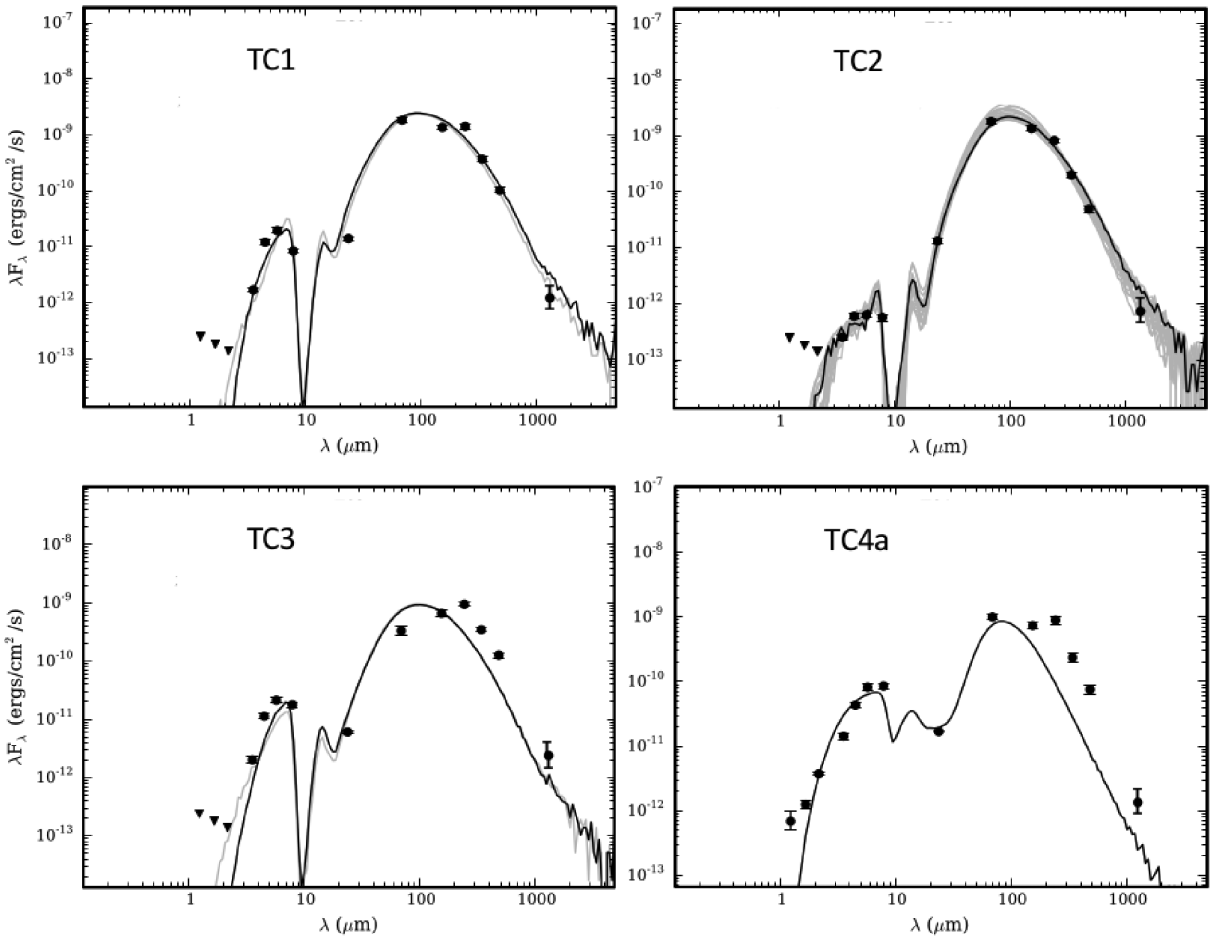

Figure 7. SEDs of the protostellar sources in the dense cores TC1, TC2, TC3, and TC4a constructed from the *JHK$_s$* CAHA photometry, *Spitzer* and *Herschel* fluxes. Central star/disc/envelope models were fitted using the tool by Robitaille et al. (2007). The best-fitting models, those with $\chi^2 - \chi^2_{\rm best}$ per data point <3, are drawn in black and grey lines. The physical parameters from the two best-fits satisfying this criterion are listed in Table 5. The 1.25-mm data are from Cernicharo et al. (1998).

Table 6. Coordinates of jet endpoints and H_2 knots in TC2 and TC4a.

Knot	α(*J*2000) h m s	δ(*J*2000) ° ′ ″	Notes
TC2			
A	18 02 28.60	−23 03 47.8	central YSO
x	18 02 28.22	−23 03 58.5	brightest knot
y	18 02 28.08	−23 04 02.2	
z	18 02 28.02	−23 04 03.9	southern H_2 tip
m	18 02 29.11	−23 03 28.6	tip of jet
n	18 02 28.81	−23 03 40.7	origin of jet
TC4a			
A	18 02 12.75	−23 05 46.7	central YSO (2.12 μm)
s	18 02 12.80	−23 05 46.2	brightest knot
x	18 02 12.73	−23 05 48.7	
z	18 02 12.72	−23 05 49.8	
w	18 02 12.95	−23 05 41.9	northern knot

the distance between the central YSO and the northern tip (m) of the visible HH 399 jet (20.4 arcsec). Also noteworthy is the fact that the H_2 knot corresponds to a local maximum in the *Herschel* emission at 70–160 μm, implying much warmer dust at this position. We point out that the near- and mid-IR source TC2-4 (Table 4), that we classify as a Class II YSO – and is also a compact radio-continuum 3.6-cm source (Lefloch et al. 2002) – has previously been suggested (Rho etal. 2006) to be the sub-millimetre counterpart to the far-IR *Herschel* source TC2. In fact, the far-IR source is extended at $\lambda > 70$ μm (Fig. 10), and has both mid-IR sources TC2-4 and 6 (see Fig. 10) within its observed peak emission. For the purpose of our model fitting, we assumed these two objects to be flux-contributors at $\lambda \simeq 8$ μm when constructing the SED from the available *Spitzer*, *Herschel*, and millimetre continuum data (see Fig. 7). The best two fits of the SED with the Robitaille et al. (2007) model (again with $\chi^2 - \chi^2_{\rm best}$ per data point <2) yield the physical parameters listed in Table 5.

3.4 The trifid condensation TC3

In common with TC0, this dense core is located practically on the edge of the H II region M 20 (see Fig. 1). This fact seems to suggest that the star formation episode that occurred inside was probably caused by the interaction of the expanding H II region into this molecular dense clump. This is the most massive core in our sample (M = 255 $M_\odot$, Table 2). Most of the detections of our near-IR survey were of moderately reddened field stars (Fig. 4). Four other sources stand out: The first (source TC3-4=A in Table 4) is located (in projection) nearly at the centre of the core, coinciding

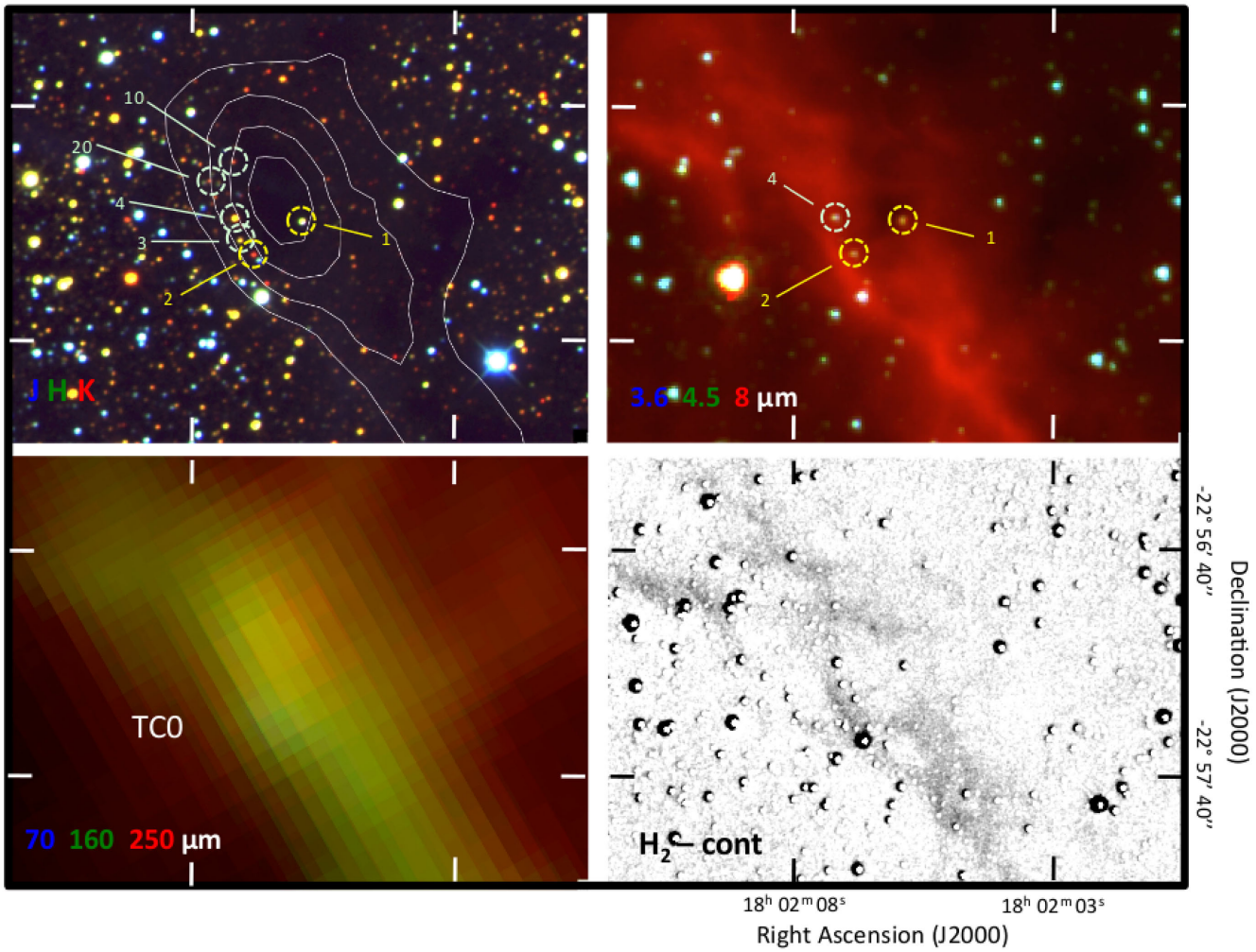

Figure 8. Close-up images of the dense clump TC0 taken with CAHA (upper left- and lowerright-hand panels), *Spitzer* (upper right-hand panel) and *Herschel* (lower left-hand panel) telescopes. The white contours on the JHK_s frame correspond to the *Herschel* 250 μm emission. The broken-line yellow circles mark the stars with near-IR colours of reddened OB stars with or without IR excesses, and broken-line cyan circles represent stars with IRAC colours of Class II objects. The size of each panel is 146 × 113 square arcsec. Labels identify sources listed in Table 4 and discussed in the text. The circular stellar residuals in the continuum-subtracted H_2 image (lower right-hand panel) are caused by the different PSFs in the two filters.

with the far-IR *Herschel* peak emission. Too faint for detection at K_s, it has the mid-IR colours of a Class I YSO. The combined *Spitzer*, *Herschel* SED (Fig. 7) of this source was analysed in a similar way as for the other Class I objects in this work (Robitaille et al. 2007). The best-fitting model parameters for this source are given in Table 5. The other three mid-IR sources (TC3-2, 8, and 10 in Table 4) are less massive Class II YSOs. As Fig. 11 shows, in this region, there is neither evidence of compact molecular hydrogen emission nor of an embedded stellar cluster.

3.5 The trifid condensation TC4

The *Herschel* images of this condensation show a segmented structure with at least three sub-condensations, named TC4a,b,c, apparently following the curved edge of the M 20 H II region. Fig. 12 shows its morphology from 1.2 to 250 μm. It is clear that TC4a is brighter and more massive than the other sub-condensations TC4b and TC4c (Lefloch & Cernicharo 2000).

3.5.1 TC4a

The *Herschel* far-IR maps of TC4a are dominated by two bright unresolved sources, labelled (following Rho et al. 2006) A and B. Source A is the most massive and coolest of the two and its physical parameters, determined from our *Herschel* images, are listed in Table 2. At the shorter wavelengths, the condensation appears to have a projected complex morphology, (see Fig. 12) as it contains at its centre a small (<20 arcsec in diameter) young star cluster consisting of one Class I (source TC4a-1=A in Table 4), four Class II YSOs (sources TC4a-4=B, TC4a-5, 7, and 8), and at least one fainter highly reddened star. We fitted the SED of the most luminous source TC4a-1=A with the model fitter of Robitaille et al. (2007), and the parameters from the best fit (only one satisfied the condition $\chi^2 - \chi^2_{\rm best}$ per data point <3) are listed in Table 5. Note that for this exercise, the flux densities at 250, 350, and 500 μm for this source were 75 per cent, 60 per cent, and 60 per cent of those reported in Table 1, respectively, to account for the unwanted contribution of the nearby compact source TC4a-4=B, which was included in the *Herschel*/SPIRE beams (>18 arcsec) at those wavelengths.

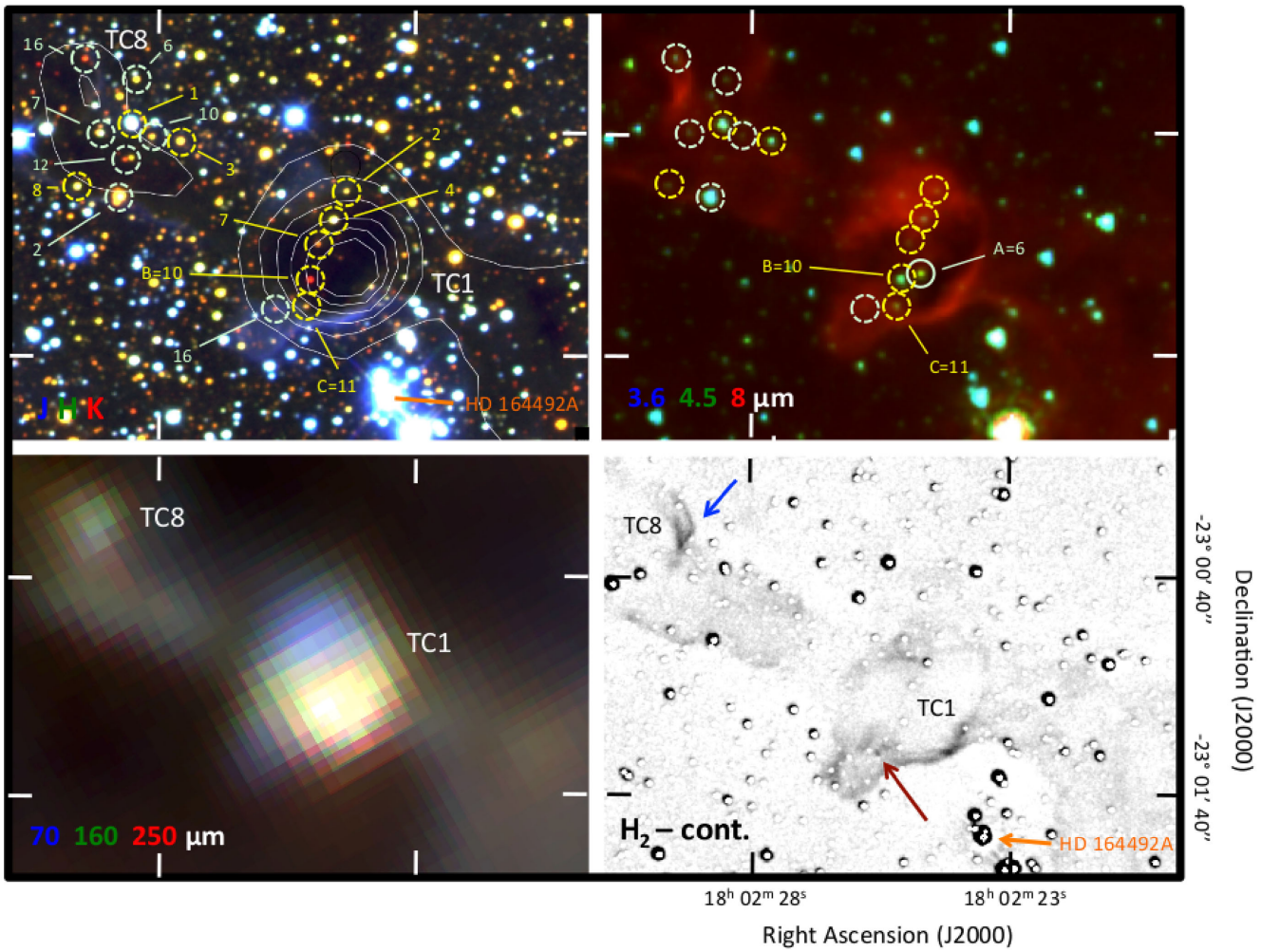

Figure 9. Close-up images of the dense clumps TC1 and TC8 taken with CAHA, *Spitzer*, and *Herschel* telescopes. The small continuous-line light cyan circle marks the sole Class 0/I source TC1-6=A. The position of the ionizing O7.5 star HD 164492A is indicated in orange. Labels identify sources listed in Table 4 and discussed in the text. Capital letters refer to the nomenclature by Rho et al. (2006). The size, scale, layout, and other symbols are as in Fig. 8. The circular stellar residuals in the continuum-subtracted H_2 image (lower right-hand panel) are caused by the different PSFs in the two filters. The red arrow marks the position of the H_2 emission compact knot discussed in Section 3.2. The blue arrow marks the position of the fan-shaped compact nebula discussed in Section 3.6.

As appreciated in Fig. 7, the fit is unsatisfactory, especially at the longer wavelengths. This is reflected by a very large value of $\chi^2 = 2300$ of the 2–10 times larger than for the other four YSOs in this study. We attribute this mainly to unaccounted contribution of the nearby compact source TC4a-4=B to the measured *Herschel*/SPIRE fluxes (at $\lambda > 250$ μm), which have larger values of the PSFs than the separation between the two sources, A and B (∼23 arcsec).

We also report the discovery of a bipolar system of H_2 emission knots associated with this YSO. Fig. 13 (lower right-hand panel) illustrates in detail its observed structure by comparing the broad-band near- and far-IR morphology with the distribution of the molecular 2.12 μm emission. Analysing this composed image (lower right-hand panel), we find several important features that are noteworthy as well as enigmatic:

(1) The near-IR morphology of object TC4a-1=A, the putative engine of the flow, is somewhat complex. As is evident in the lower right-hand panel of Fig. 13, the centroid of its unresolved emission shifts up to 0.6 arcsec, towards the SE with increasing wavelength, from 1.2 to 2.2 μm. We interpret this as indication of the presence of a small dust structure (possibly a disc) around the YSO A that would be responsible for the 18 K dust emission (Table 2).

(2) In the H_2 continuum-subtracted image (lower left-hand panel of Fig. 13), we find two symmetric series of compact H_2 emission knots separated by 4.1 arcsec with a position angle of 21 °, at whose midpoint, a bright, roundish molecular hydrogen nebula (1.6 arcsec in diameter) is located. The centre of this structure is separated by 0.8 arcsec from the YSO at 2.2 μm. The system is reminiscent of the Burnham nebula close to T Tauri (cf. van Langevelde et al. 1994). High-resolution spectroscopy in the 2.12 μm line emission (ideally with proper motion data) is required to study the kinematics of this outflow.

A second bright *Herschel* mid- and far-IR source (TC4a-4=B in Table 4 and Fig. 12) is located some 23 arcsec south of YSO TC4a-1=A. Being too faint to be detected in the near-IR, its nature is difficult to assess. Its IRAC colours (cf. Fig. 6) suggest a bright 4.5 μm-channel contribution, possibly dominated by the Br α line, as no trace of molecular hydrogen emission is seen at 2.12 μm. Its

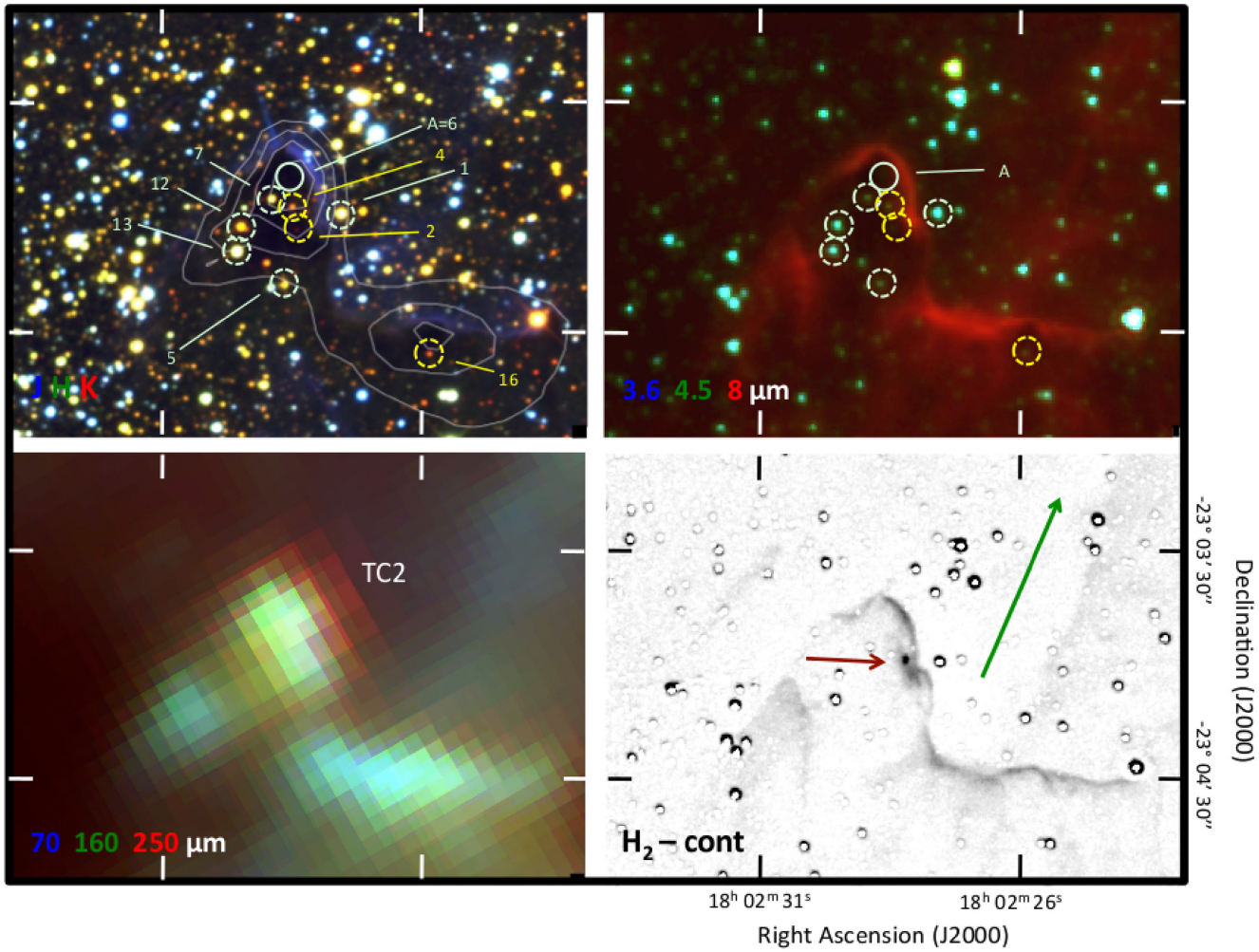

Figure 10. Close-up images of the dense clump TC2 taken with CAHA, *Spitzer*, and *Herschel* telescopes. The small continuous-line light cyan circle marks the sole Class 0/I *Spitzer* source TC2-6=A. Labels identify sources listed in Table 4 and discussed in the text. Capital letters refer to the nomenclature by Rho et al. (2006). The size, scale, layout, and other symbols are as in Fig. 9. The circular stellar residuals in the continuum-subtracted H_2 image (lower right-hand panel) are caused by the different PSFs in the two filters. The green arrow points towards the ionizing star HD 164492A.

SED suggests a lower dust mass and a lower dust temperature than that of source A.

3.5.2 TC4b and TC4c

These two sub-condensations, identified and named by Lefloch & Cernicharo (2000), are fainter millimetre far-IR sources lying along the SW filament and their derived masses are 10–20 per cent of that of TC4a and have approximately the same age (Rho et al. 2006; Lefloch et al. 2008). The fragmentation and star formation processes may have been triggered by the expansion of the H II regions (Lefloch & Cernicharo 2000).

Our near- and mid-IR surveys reveal a small number of unresolved sources in each of these cores. In the case of TC4b, we have found two IRAC sources that have the mid-IR colours of Class I protostars: sources TC4b-2=D and TC4b-6. Both lie, within the *Herschel* resolution, even at 70 μm, at the peak dust-emission, namely $\alpha(J2000) = 18^{h}02^{m}14\overset{s}{.}3$, $\delta(J2000) = -23°06'35''6$. Source TC4b-6 is fainter and redder in the IRAC bands (Table 4, Fig. 6), and undetected at $\lambda < 3$ μm. Additionally, three Class II sources were identified in the vicinity, whereas in TC4c, only two Class II sources were found.

As can be seen in the lower left-hand panel of Fig. 12, the dust emission from these subcondensations is extremely faint, particularly at the shortest *Herschel* wavelengths. This precluded us from constructing meaningful SEDs, and, thus, from estimating dust parameters.

3.6 TC8

It is not clear whether TC8 is a separate dense core or just an extension of TC1. In any case, it appears (see Fig. 1) that this condensation belongs to the same dense filament extending towards the east. The observed far-IR and millimetre emission is centrally peaked, implying a considerably lower dust mass than TC1 (Lefloch et al. 2008). The apex of a fan-shaped nebular PAH- and (probably luminisent) H_2-line emission appears to emerge from the densest part of the globule (Fig. 9), but the near-IR photometry of the compact sources in its vicinity does not reveal any bright very young (Class I) stellar object (Table 4 and Fig. 4). There are, nevertheless,

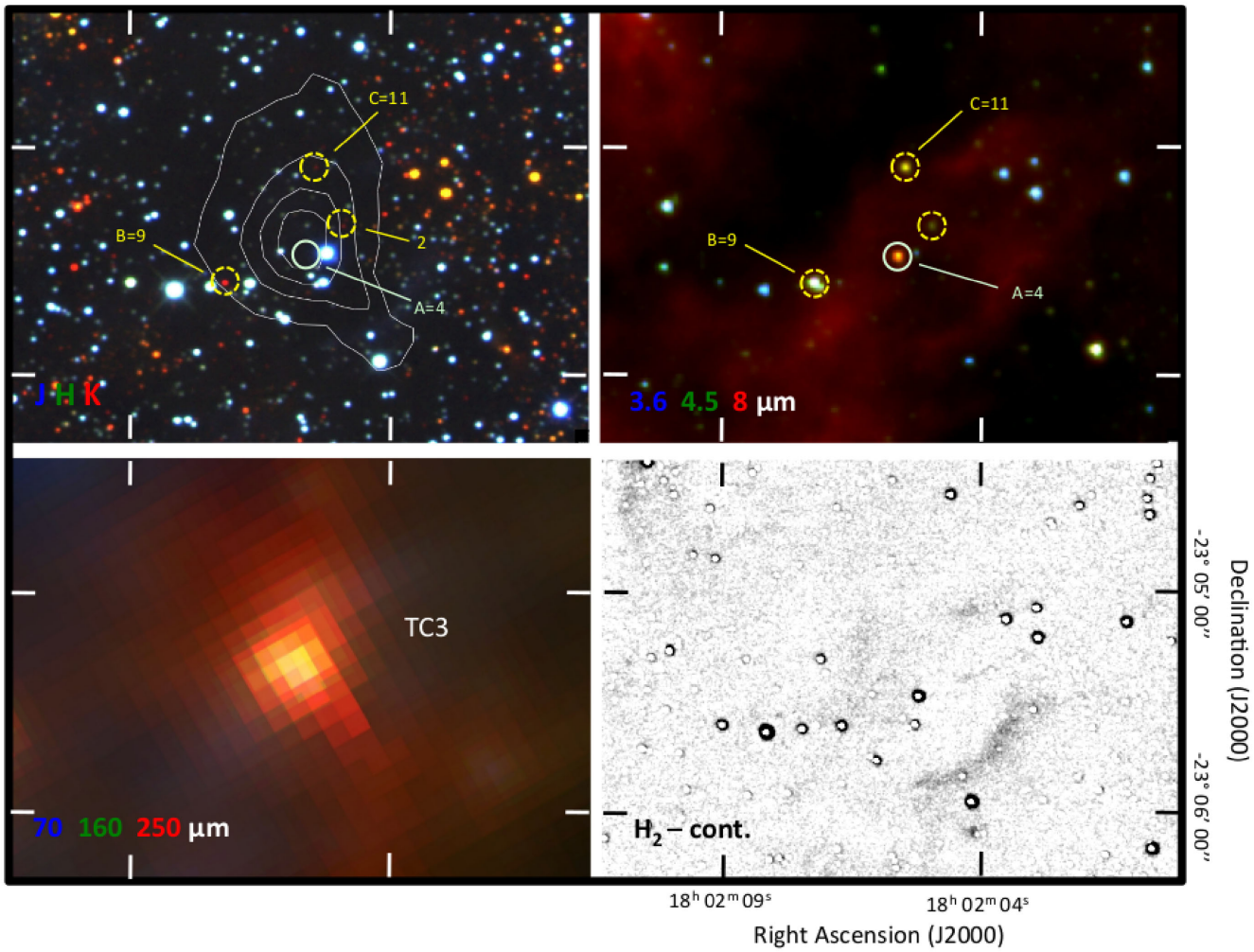

Figure 11. Close-up images of the dense clumps TC3 taken with CAHA, *Spitzer*, and *Herschel* telescopes. The small continuous-line light cyan circle marks the sole Class 0/I *Spitzer* source TC3-4=A. Labels identify sources listed in Table 4 and discussed in the text. Capital letters refer to the nomenclature by Rho et al. (2006). The size, scale, layout, and other symbols are the same as in Fig. 9. The circular stellar residuals in the continuum-subtracted H_2 image (lower right-hand panel) are caused by the different PSFs in the two filters.

a number of embedded OB stars and low mass Class II sources in the region.

4 FINAL REMARKS AND CONCLUSIONS

4.1 Multistage star formation

The observations presented in this work support the concept, previously put forward, that M 20 has been subjected to multiple episodes of star formation (see review by Rho et al. 2008). These results describe in detail what appears to be the most recent of such events occurring in the most massive dense clumps located both at the edges of the expanding H II region (TC0, TC3, and TC4a,b,c), where the ionized gas encounters denser material and where the stellar ultraviolet (UV) radiation has been geometrically diluted (for a discussion, see Cernicharo et al. 1998). Simultaneous formation of stars appears to be occurring in dense clumps close to the nebula's (projected) centre, in regions (PDRs) subject to very heavy UV illumination (TC1, TC2, and TC8). These occur along well-defined molecular filaments. In all cases, the collapse in the clumps results only in the formation of low- or intermediate-mass stars. No clear evidence is found that some or all of these events have been triggered by the previous massive star formation episode that created HD 164492, but the influence of these massive stars on the ambient conditions must have played a major role.

4.2 Main conclusions

From the analyses of our 1 to 500 μm observations of the central dense condensation (TC0, TC1, TC2, TC3, TC4a,b,c, and TC8) in the central region of the Trifid nebula, we derive the following conclusions:

(1) Re-analysis of the available optical and near-IR photometry, and spectroscopy of the early-type trapezium-type system, HD 164492 that ionizes the M 20 H II region, led to a revised value of the distance to this nebula of $d = 2.0 \pm 0.1$ kpc, which is 19 per cent larger than the one that has been generally assumed.

(2) Seven of the eight observed TCs show embedded Class II YSOs. The far-IR emission of five of them is dominated by Class I

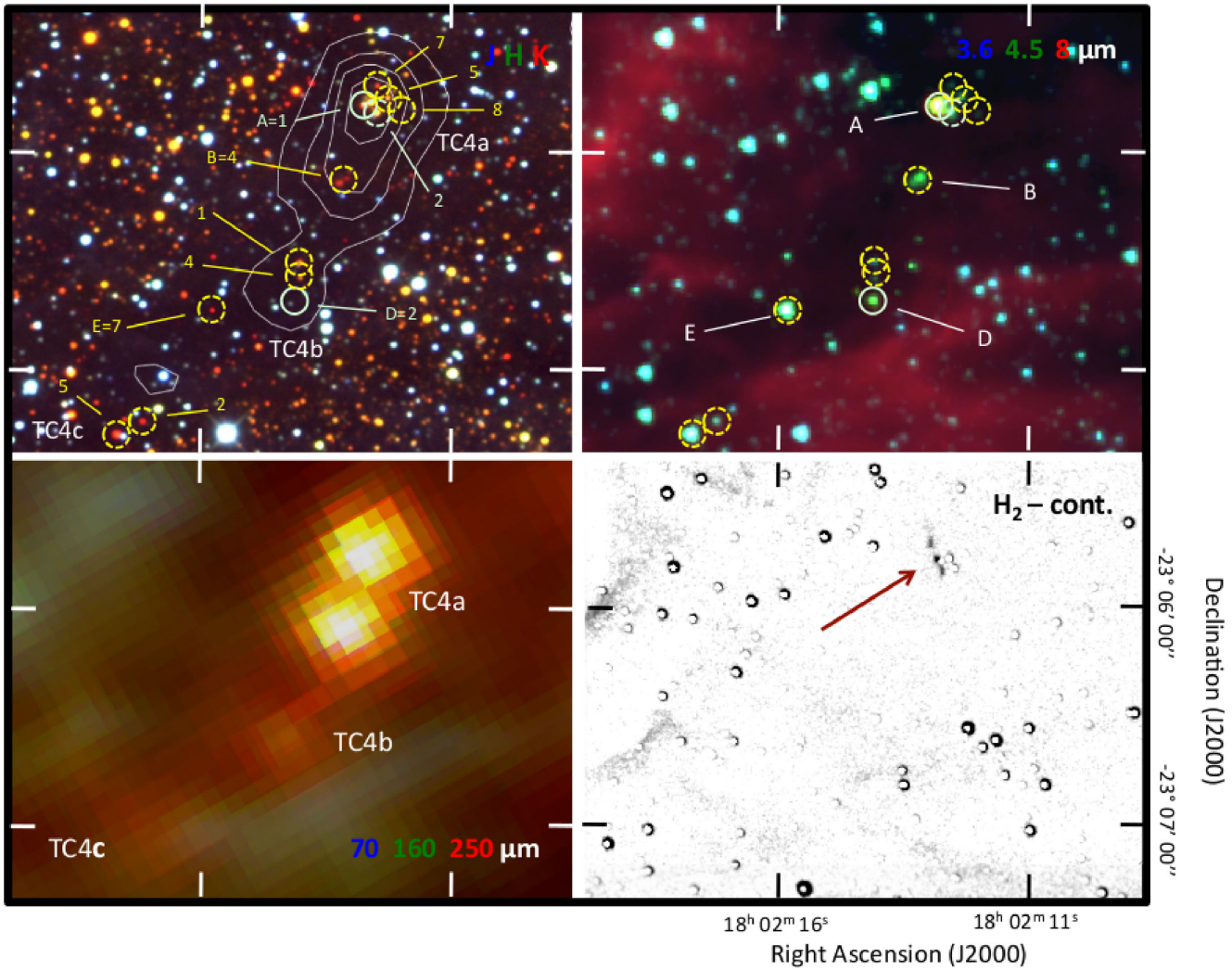

Figure 12. Close-up images of the dense clumps TC4a,b,c (nomenclature by Lefloch & Cernicharo 2000) taken with CAHA, *Spitzer*, and *Herschel* telescopes. The small continuous-line light cyan circles mark the Class 0/I *Spitzer* sources TC4a-1 and TC4b-2=D. Labels identify sources listed in Table 4 and discussed in the text. Capital letters refer to the nomenclature by Rho et al. (2006). The size, scale, layout, and other symbols are the same as in Fig. 9. The circular stellar residuals in the continuum-subtracted H_2 image (lower right-hand panel) are caused by the different PSFs in the two filters.

protostars near the (projected) centre of the cores. Only TC0 appears void of embedded YSOs.

(3) The derived total masses of the most luminous five cores, TC0, TC1, TC2, TC3, and TC4a, range between 50 and 250 $M_\odot$, with average dust temperatures between 13 and 19 K. The total luminosities of their embedded protostars were found to be in the range between 80 and 570 $L_\odot$.

(4) Evidence of energetic outflows is found in three cores, TC1, TC2, and TC4a, that show small molecular hydrogen knots, most probably excited by shocks. TC1 and TC2 are star-forming PDRs illuminated by the O7.5 luminous star HD 164492 in the centre of M 20. In TC2, we report the presence of an H_2-emitting probable counterjet to the well-known optical and IR Herbig–Haro object HR 399 and a new candidate for the central protostellar engine. In the centre of TC4a, we discovered an aligned triplet of H_2 emission knots with a Class I YSO at their central position, strongly suggesting that this could be the result of an energetic bipolar outflow.

(5) Although far from being conclusive, the present results support the idea that M 20 is a good example of massive star-forming region in a turbulent, filamentary molecular cloud, where star formation has been active for at least 3×10^5 yr, the typical lifetime of Class II sources.

ACKNOWLEDGEMENTS

We acknowledge the anonymous referee for a very thorough and detailed revision of the original manuscript. Her/his comments and suggestions led to a significant improvement in the clarity of the paper. The results presented in this paper are based on observations made with the 3.5-m telescope of Calar Alto Observatory and with *Herschel*, which is an ESA space observatory with science instruments provided by European-led Principal Investigator consortia and with important participation from NASA. This paper makes use of archival data obtained with the *Spitzer Space Telescope*, which is operated by the Jet Propulsion Laboratory, California Institute of Technology (CIT) under National Aeronautics and Space Administration (NASA) contract 1407. MT and CR-Z acknowledge financial support from UNAM/PAPIIT grants Nos IN-104316 and IN-108117.

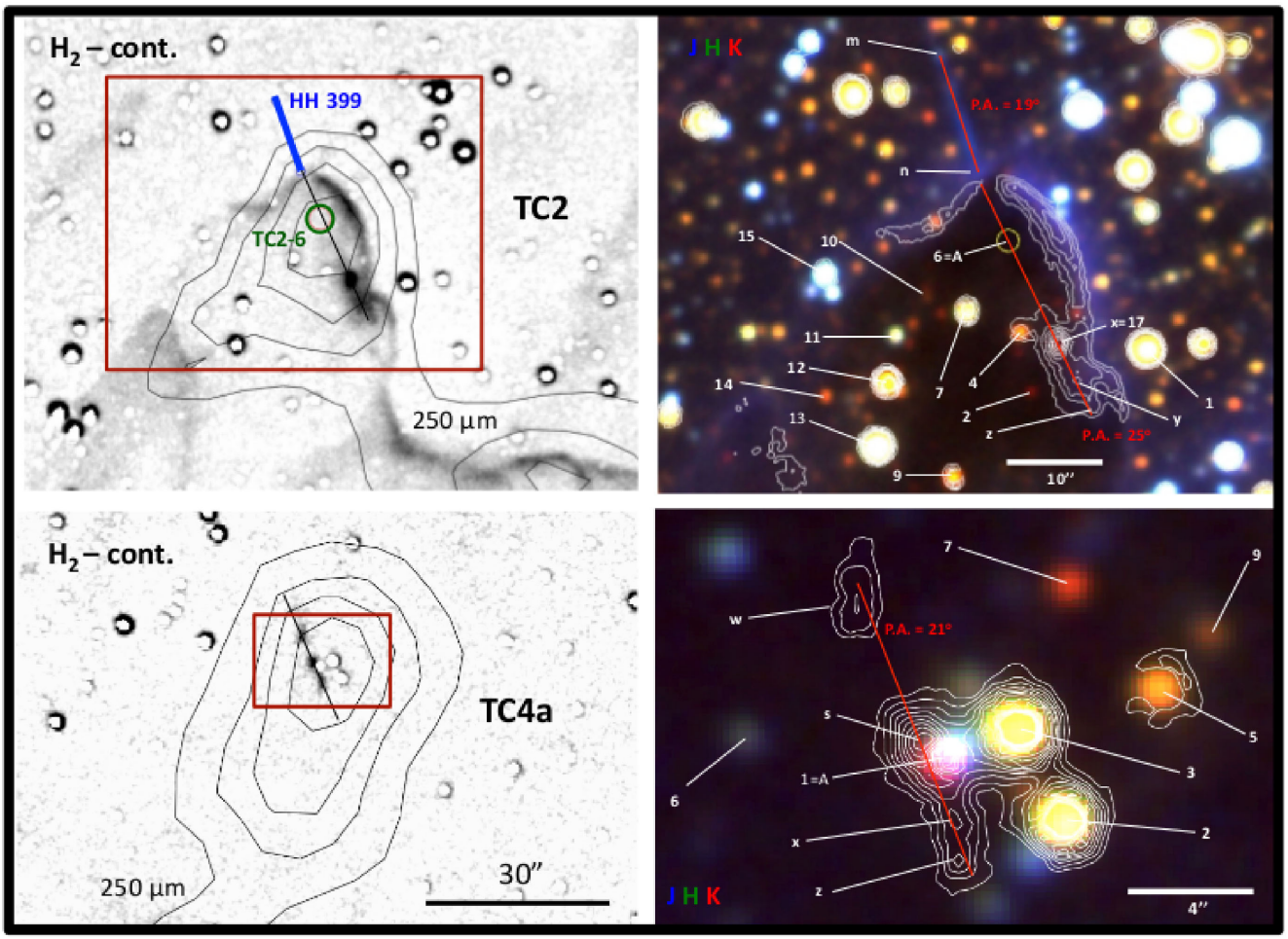

Figure 13. Magnified views of two regions where new shocked molecular hydrogen emission knots are discovered, TC2 and TC4a (upper and lower panels, respectively). On the left, the *Herschel* 250 μm emission contours are plotted over the continuum-subtracted molecular hydrogen line (2.12 μm) emission images. The straight thin black lines at 23° position angles join the jet and H_2 knots with the putative central driving sources, TC2-6 and TC4a-1. The blue line represents the HH 399 optical and near-IR jet. Panels on the right show close-up sections (marked with dark red rectangles on the left-hand panels) of the JHK_s images showing the details of the jets. White contours represent the continuum-subtracted 2.12 μm H_2 emission. The reddest near- and mid-IR sources are labelled with numbers as in Table 4. The letters identify the small H_2 knots and the endpoints of HH 399, all listed in Table 5. Red lines (with corresponding position angles) mark the direction of the proposed flows (see text). The coordinates of TC2-6=A are: $\alpha(J2000) = 18^h02^m28\overset{s}{.}6$, $\delta(J2000) = -23°03'48''$, and those of TC4-1 = A are $\alpha(J2000) = 18^h02^m12\overset{s}{.}8$, $\delta(J2000) = -23°05'47''$. North is at the top, east to the left. Spacial scales are illustrated with horizontal bars

REFERENCES

Benjamin R. A. et al., 2003, PASP, 115, 953
Bertin E., Arnouts S., 1996, A&AS, 117, 393
Cernicharo J. et al., 1998, Science, 282, 462
Chaisson E. J., Wilson R. F., 1975, ApJ, 199, 647
Elia D. et al., 2013, ApJ, 772, 45
Elia D. et al., 2017, MNRAS, 471, 100
Fazio G. et al., 2004, ApJS, 154, 10
Giannini T. et al., 2012, A&A, 539, A156
Hester J. J., Desch S. J., Healy K. L., Leshin L. A., 2004, Science, 304, 1116
Hiltner W. A., 1956, ApJS, 2, 389
Kohoutek L., Mayer P., Lorenz M., 1999, A&AS, 134, 129
Kovacs Z., Mall U., Bizenberger P., Baumeister H., R"oser H.-J., 2004, in James D. G., James W. B., eds, Proc. SPIE Conf. Ser. Vol. 5499, Optical and Infrared Detectors for Astronomy. SPIE, Bellingham, p. 432
Lefloch B., Cernicharo J., 2000, ApJ, 545, 340
Lefloch B., Cernicharo J., Rodríguez L. F., Miville-Deschenes M. A. Cesarky D., 2002, ApJ, 581, 335
Lefloch B., Cernicharo J., Pardo J. R., 2008, A&A, 489, 157
Levine J., 2008, PhD Thesis, Univ. Florida
López-Chico T. A., Salas L., 2007, Rev. Mex. Astron. Astrofis., 43, 155
Lynds B. T, Canzian B. J., O'Neal E. J., 1985, ApJ, 294, 578
Martins F., Schaerer D., Hillier D. J., 2005, A&A, 436, 1049
Meyer M. R., Calvet N., Hillebrand L. A., 1997, AJ, 114, 288
Molinari S. et al., 2010, A&A518, L100
Molinari S. et al., 2016, A&A, 591, A149
Pecaut M. J., Mamajet E. E., 2013, ApJS, 208, 9
Pilbratt G. L. et al., 2010, A&A, 518, L1
Raga A., Cantó J., 1995, Rev. Mex. Astr. Astrofis., 31, 51
Rho J., Ramirez S. V., Corcoran M. F., Hamaguchi K., Lefloch B., 2004, ApJ, 607, 904
Rho J., Reach W., Lefloch B., Fazio G., 2006, ApJ, 643, 965
Rho J., Lefloch B., Reach W. T., Cernicharo J., 2008, in Reipurth B., ASP Conf. Ser. Vol. 5, Handbook of Star Forming Regions. Astron. Soc. Pac., San Francisco, p. 509
Rieke G. H., Lebofsky M. J., 1985, ApJ, 288, 618
Robitaille T. P., Whitney B. A., Indebetouw R., Wood K., Denzmore P., 2006, ApJS, 167, 256

Robitaille T. P., Whitney B. A., Indebetouw R., Wood K., 2007, ApJS, 169, 328
Román-Zúñiga C. G., 2006, PhD Thesis, Univ. Florida
Rosado M., Esteban C., Lefloch B., Cernicharo J., García-López R. J., 1999, AJ, 118, 2962
Siess L., Dufour E., Forestini M., 2000, A&A, 358, 599
Stetson P. B., 1987, PASP, 99, 191
Stone R. C., 1978, AJ, 83, 393
Strutskie et al., 2006, AJ, 131, 1163
Tapia M., 1981a, MNRAS, 197, 949
Tapia M., 1981b, PhD Thesis, Univ. Edinburgh
Tapia M., Roth M., Marraco H., Ruiz M. T., 1988, MNRAS, 232, 661
Tapia M., Persi P., Roth M., Elia D., Molinari S., Saldaño H. P., Gómez M., 2014, MNRAS, 437, 606
Tokunaga A. T., 2000, in Arthur N., ed, Allen's Astrophysical Quantities, 4th ed. Am. Inst. Phys., New York, p. 143
Traficante A. et al., 2011, MNRAS, 416, 2932
van Langevelde H. J., van Dishoeck E. F., van der Werf P. P., Blake G. A., 1994, A&A, 287, L25
Walborn N. R., 1973, AJ, 78, 1067
Werner M. et al., 2004, ApJS, 154, 1
Ybarra J., Tapia M., Román-Zúñiga C., Lada E., 2014, ApJ, 794, L25
Yusef-Zadeh F., Shure M., Wardle M., Kassim N., 2000, ApJ, 540, 842
Yusef-Zadeh F., Biretta J., Geballe T. R., 2005a, AJ, 130, 1171
Yusef-Zadeh F., Biretta J., Wardle M., 2005b, ApJ, 624, 246

This paper has been typeset from a TEX/LATEX file prepared by the author.